Biomedicine & Pharmacotherapy 175 (2024) 116726

Contents lists available at ScienceDirect

Biomedicine & Pharmacotherapy

journal homepage: www.elsevier.com/locate/biopha

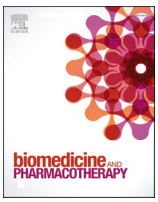

Preclinical development of humanized monoclonal antibodies against CD169 as a broad antiviral therapeutic strategy

Patricia Resa-Infante [a,b,c,d,*], Itziar Erkizia [a], Xabier Muñiz-Trabudua [a], Federica Linty [e,f], Arthur E.H. Bentlage [e,f], Daniel Perez-Zsolt [a], Jordana Muñoz-Basagoiti [a,1], Dàlia Raïch-Regué [a], Nuria Izquierdo-Useros [a], Theo Rispens [e,g,h], Gestur Vidarsson [e,f], Javier Martinez-Picado [a,b,c,d,i,*]

[a] IrsiCaixa, Hospital Germans Trias i Pujol, Badalona 08916, Spain
[b] University of Vic-Central University of Catalonia (UVic-UCC), Vic 08500, Spain
[c] Germans Trias i Pujol Research Institute (IGTP), Can Ruti Campus, Badalona 08916, Spain
[d] CIBERINFEC, Madrid 28029, Spain
[e] Sanquin Research, Amsterdam 1066 CX, the Netherlands
[f] Utrecht Institute for Pharmaceutical Sciences and Bijvoet Center for Biomolecular Research, Utrecht University, Utrecht 3584 CH, the Netherlands
[g] Landsteiner Laboratory, Amsterdam University Medical Center, Amsterdam 1066 CX, the Netherlands
[h] Amsterdam Institute for Infection and Immunity, Amsterdam, the Netherlands
[i] Catalan Institution for Research and Advanced Studies (ICREA), Barcelona 08010, Spain

ARTICLE INFO

Keywords:
Antibody therapy
Antivirals
Humanization
Methods
Monoclonal antibody

ABSTRACT

New therapies to treat or prevent viral infections are essential, as recently observed during the COVID-19 pandemic. Here, we propose a therapeutic strategy based on monoclonal antibodies that block the specific interaction between the host receptor Siglec-1/CD169 and gangliosides embedded in the viral envelope. Antibodies are an excellent option for treating infectious diseases based on their high specificity, strong targeting affinity, and relatively low toxicity. Through a process of humanization, we optimized monoclonal antibodies to eliminate sequence liabilities and performed biophysical characterization. We demonstrated that they maintain their ability to block viral entry into myeloid cells. These molecular improvements during the discovery stage are key if we are to maximize efforts to develop new therapeutic strategies. Humanized monoclonal antibodies targeting CD169 provide new opportunities in the treatment of infections caused by ganglioside-containing enveloped viruses, which pose a constant threat to human health. In contrast with current neutralizing antibodies that bind antigens on the infectious particle, our antibodies can prevent several types of enveloped viruses interacting with host cells because they target the host CD169 protein, thus becoming a potential pan-antiviral therapy.

1. Introduction

Enveloped viruses constitute a permanent threat to global health, as observed during the human immunodeficiency virus (HIV-1) pandemic, the Ebola virus (EBOV) outbreaks, and, more recently, the COVID-19 pandemic caused by the coronavirus SARS-CoV-2. While antigen-presenting cells of myeloid lineage, such as monocytes, macrophages, and dendritic cells (DCs), are essential for recognizing foreign pathogens and triggering the innate and adaptive immune responses, some viruses exploit host-protective strategies to disseminate within the organism through lymphoid tissues. For instance, they utilize sialic acid–binding Ig-like lectin 1 (CD169/Siglec-1), a *trans*-membrane protein expressed in

Abbreviations: Cat. no., catalogue number; CD169/Siglec-1, sialic acid–binding Ig-like lectin 1; CDR, complementarity-determining region; DCs, dendritic cells; EBOV, Ebola virus; FRs, framework residues; HIV-1, human immunodeficiency virus; IC_{50}, half maximal inhibitory concentration; MAbs, monoclonal antibodies; VH, variable regions from heavy chain of antibody; VL, variable regions from light chain of antibody; VLP, virus-like particle.

* Corresponding authors at: IrsiCaixa, Hospital Germans Trias i Pujol, Badalona 08916, Spain.
E-mail addresses: prinfante@irsicaixa.es (P. Resa-Infante), jmpicado@irsicaixa.es (J. Martinez-Picado).
[1] Current affiliation: Centre de Recerca en Sanitat Animal (CReSA), Campus de la Universitat Autònoma de Barcelona (UAB), Bellaterra, Spain.

https://doi.org/10.1016/j.biopha.2024.116726
Received 16 January 2024; Received in revised form 30 April 2024; Accepted 6 May 2024
Available online 15 May 2024

DCs and other myeloid cells as an attachment receptor mediating the uptake of enveloped viruses into DCs and contributing to their dissemination throughout the host [15,23,25–27]. This interaction involves the recognition of sialyllactose in gangliosides embedded in cellular membranes, which that are dragged by HIV-1 and other enveloped viruses when they bud from the plasma membrane of infected cells [16]. Since antibody therapy is the predominant class among recently developed drugs because of its high specificity, low toxicity, and extraordinarily successful development [19], we propose a therapeutic strategy to block the specific interaction between CD169 and gangliosides embedded in the viral envelope. This strategy consists of administering monoclonal antibodies (mAbs) that bind the ligand-recognition domain of CD169 to block entry of enveloped viruses. Initially, we developed a batch of five mAbs in mice and proved their efficacy for preventing attachment of HIV-1 and EBOV to host myeloid cells [23]. We have since humanized three of them to reduce immunogenicity against mouse protein sequences in humans. Moreover, we have optimized these new antibodies to eliminate potential sequence liabilities that could generate antibody-relevant instabilities during production and storage and, thus, to increase their chemical stability. We performed functional assays to demonstrate that, after the humanization process that converts the antibodies into human IgG1 mAb, they maintain their capacity to block i) HIV-1 uptake and *trans*-infection, ii) EBOV uptake and viral fusion, and iii) SARS-CoV-2 uptake and *trans*-infection from antigen-presenting cells, further proving their potential therapeutic application for prevention and/or treatment of viral infectious disease. Finally, we performed in-depth biophysical characterization of our humanized mAbs under normal conditions and under oxidative stress and found that optimized humanized mAb retains a strong affinity for and specificity to CD169.

2. Material and methods

2.1. Ethics and biosafety statements

The study was approved by the institutional review board for biomedical research of Hospital Germans Trias i Pujol (HUGTiP).

The biosafety committee of the Germans Trias i Pujol Institute approved the performance of SARS-CoV-2 experiments at the BSL3 laboratory of the Center for Bioimaging and Comparative Medicine (CSB20–015-M7).

2.2. Antibody cloning

Total RNA isolated from hybridomas was reverse-transcribed into cDNA using isotype-specific anti-sense primers or universal primers following the technical manual of the PrimeScript™ 1st Strand cDNA Synthesis Kit. The antibody fragments of VH, VL, CH, and CL were amplified according to the standard operating procedure for rapid amplification of the cDNA ends (RACE) of GenScript and followed by sequence analysis.

VH and VL of murine antibodies were aligned using Ig Blast-NCBI (https://www.ncbi.nlm.nih.gov/igblast) to generate the closest related human V gene sequences and to identify the framework residues (FRs) and complementarity-determining regions (CDRs). For the humanization process, mouse residues forming the CDRs were retained, while FRs not matching between mouse and human germlines were changed to the residue present in the human V gene.

Constructs with the murine VH and VL sequences of #1F5, #3F1, and #5B10 antibodies (Invitrogen) were used to produce each antibody following an approach applied elsewhere [7] as both mouse/human chimeric hIgG1 and humanized CDR-engrafted hIgG1. For the light chain, constructs encoding the whole light chain (VL + CL) (Invitrogen) were cloned into the pcDNA3.1 mammalian expression vector. For the heavy chain, constructs encoding the VH flanked by the *Hin*dIII and *Nhe*I restriction sites (Invitrogen) were cloned into the pMA-RQ vector. Each VH was excised from the pMA-RQ vector by digestion of *Hin*dIII and *Nhe*I and cloned into a pcDNA3.1 vector that already contained the human IgG1 constant domains [7]. DNA encoding anti-CD169 variants was applied to remove potential sequence liabilities. This was ordered directly from the manufacturer (Invitrogen) or generated by site-directed mutagenesis. All constructs were amplified by maxiprep and sequenced for validation. Plasmids can be made available by contacting the corresponding author. Use of the plasmids and sequence information is for non-commercial purposes only.

2.3. Antibody production

Suspensions growing HEK FreeStyle™ 293-F cells (cat. no. R790–07, ThermoFisher Scientific) were cultured in FreeStyle™ 293 Expression Medium (cat. no. 12338026, ThermoFisher Scientific) at 37°C with 8% CO_2 as described elsewhere [7]. On the day of transfection, cells were centrifuged and seeded at a density of 1E6 cells/ml in fresh Freestyle medium. Plasmids encoding the heavy and kappa chains of each antibody were transiently transfected using PEI (polyethylenimine; Ref. 24765–1, Polysciences Inc.), together with 3 helper plasmids (pORF21, pORF27, and p33-SV40LT) [32]. Transfection mixtures per 100 ml of cell culture contained 31.4 μg of heavy chain construct, 37.7 μg of light chain construct, 31 μg of helper vector mix, 300 μg of PEI, and 6 ml of optiMEM (cat. no. 51985026, ThermoFisher Scientific). Transiently transfected HEK293FS cells were cultured at for 6 days at 37°C in 8% CO_2. The culture medium was harvested by centrifugation, and the antibodies were purified from the culture medium using Protein A HiTrap columns (ThermoFisher Scientific) and eluted using citrate buffer (20 mM citrate, 150 mM NaCl, pH=3.5), followed by neutralization with phosphate buffer (KH_2PO_4/K_2HPO_4 pH=8). The buffer was transformed into 5% glucose, 5 mM sodium acetate, pH 4.5, using Pierce Protein Concentrator PES, 10 kDa (cat. no. 88517, Pierce). The antibody concentration was determined by measuring absorbance at 280 nm. Volume was adjusted to ensure that each antibody was at 1 mg/ml.

2.4. Prediction of sequence liabilities

The structure-based antibody prediction server SAbPred (http://opig.stats.ox.ac.uk/webapps/sabpred) was used to identify potential sequence liabilities [8]. A literature search was then performed to identify liabilities that have already proven to have a negative impact during the manufacture of biological drugs [3,4,12,18,22,28,33].

2.5. Functional competition assay with Raji-Siglec-1 cells

A Raji-Siglec-1 cell line was generated in our laboratory to constitutively express the CD169 receptor as described previously [23]. This cell line was maintained in RPMI media (cat. no. 21875091, Gibco, Thermo Invitrogen) supplemented with 1 mg/ml of geneticin (cat. no. 10131–027, Gibco, Thermo Invitrogen), 10% FBS (cat. no. 10270–106, Gibco, Thermo), 100 IU/ml of penicillin, and 100 μg/ml of streptomycin (cat. no. 15070063, Gibco, Thermo).

HEK-293 T/17 cells (cat. no. CRL-11268, ATCC repository) were cultured in DMEM (cat. no. 41966–029, Gibco, Thermo Invitrogen) supplemented with 10% FBS, 100 U/ml of penicillin, and 100 μg/ml of streptomycin at 37°C with 8% CO_2. $HIV_{Gag\text{-}eGFP}$ VLP stocks were generated by transfecting 1E7 HEK-293 T/17 cells with 15 μg of pHIV-Gag-eGFP plasmid using 15 μl of LipoD293 (Ver. II) reagent (cat. no. SL100668, SignaGen). Supernatants containing VLPs were filtered (Millex HV, 0.45 μm; Millipore) and frozen at −80°C until use.

Serial dilutions ranging from 20 μg/ml to 0.2 μg/ml of anti-CD169 antibodies or IgG1 isotype control (cat. no. 554721, BD Bioscience) were prepared in supplemented RPMI media. Then, $HIV_{Gag\text{-}eGFP}$ VLPs were added at a non-saturating concentration, followed by Raji-Siglec-1 cells. The assay was run for 60 min at 37°C. After washing with PBS, cells were suspended in PBS supplemented with 0.5% FBS and analyzed by

FACS (FACSCantoII, BD) to determine VLP uptake and (analyzed with FlowJo software (Fig S1). As non-inhibiting controls, we used the corresponding mAb isotype controls, while as a negative control, we used cells not exposed to the virus particles. All experiments were performed in duplicate. The IC_{50} derived from this procedure depends on the assay conditions and cannot be readily compared between experiments not performed simultaneously.

2.6. Generation of viral stocks

To generate HIV-$1_{NL4.3\ Gag\text{-}iGFP}$ stocks, 1E7 HEK-293 T/17 cells (cultured as previously described) were transfected with 20 μg of pHIV-Gag-iGFP plasmid using XtremeGene9 reagent (cat. no. 6365809001, MERCK) following the manufacturer's instructions. Supernatants containing VLPs were collected 48 hours post-transfection, filtered (Millex HV, 0.45μm; Millipore), and frozen at −80°C until use.

To generate HIV-1_{NL4-3}, 1E7 HEK-293 T/17 cells (cultured as previously described) were transfected with 30 μg of pNL4–3 plasmid—obtained from the US National Institute of Health (NIH) AIDS Research and Reference Reagent Program—using a calcium phosphate kit (Calphos; Clontech) and following the manufacturer's instructions. Supernatants containing viral particles were collected 48 hours post-transfection, filtered (Millex HV, 0.45μm; Millipore), and frozen at −80°C until use. The $p24^{Gag}$ content of HIV-$1_{NL4-3\ Gag\text{-}iGFP}$ VLPs and HIV-1_{NL4-3} viral stocks was determined using enzyme-linked immunosorbent assay (ELISA) (Perkin-Elmer) for titration of viral preparations.

$EBOV_{eGFP\text{-}VP40}$ and $EBOV_{BlaM\text{-}VP40}$ VLPs were generated as described elsewhere [23]. $EBOV_{eGFP\text{-}VP40}$ VLPs were generated by transfecting HEK-293 T/17 cells with the molecular clone CAGGS-eGFP-VP40 (kindly provided by Dr. Bieniasz). In the case of $EBOV_{BlaM\text{-}VP40}$ VLPs, cells were transfected with the molecular clones pcDNA3.1-BlaM-VP40, pcDNA3-Zaire-NP, and pcDNA3.1-Zaire-GP (all from BEI Resources). Supernatants containing VLPs were collected 72 h post-transfection. The supernatants were clarified by centrifugation at 720xg for 10 min and frozen at −80°C until use. The $EBOV_{VP40}$ content of $EBOV_{eGFP\text{-}VP40}$ and $EBOV_{BlaM\text{-}VP40}$ VLP stocks was determined using an in-house ELISA assay with anti-VP40 IgG1 antibody (cat. no. 10–2351, Fitzgerald) and rVP40 protein (cat. no. 0564–001, IBT Bioservices) as standard controls. Capture antibody was prepared at 500 ng/ml, and 100 μl per well was incubated in 96-well plates (Nunc MaxiSorp) for 16 h.

SARS-CoV-2 was isolated in March 2020 from a nasopharyngeal swab as described elsewhere (Rodon, 2021). The virus was propagated by making two passes through Vero E6 cells. The genomic sequence was deposited in the GISAID repository with accession ID EPI_ISL_510689 (http://gisaid.org). Vero E6 cells (ATCC CRL-1586) were cultured in DMEM medium supplemented with 5% FBS, 100 U/ml penicillin, 100 μg/ml streptomycin, and 2 mM glutamine (ThermoFisher Scientific). TMPRSS2/ACE2 HEK-293 T cells used were generated by transiently transfecting TMPRSS2 human plasmid (Origene) with X-tremeGENE HP Transfection Reagent (cat. no. 6365809001, Merck) into the ACE2 HEK-293 T cell line. This cell line, which constitutively over-expresses human ACE2 protein, was kindly provided by Integral Molecular Company. TMPRSS2/ACE2 HEK-293 T cells were maintained in DMEM supplemented with 10% FBS, 100 IU/ml penicillin, 100 μg/ml streptomycin, 1 μg/ml puromycin (Invitrogen), and 1 mg/ml geneticin (Invitrogen).

2.7. Viral entry into primary myeloid cells

Peripheral blood mononuclear cells from blood donors were obtained using Ficoll-Hypaque density gradient centrifugation (cat. no. 1114547, ATOM). Then, monocyte populations (>97% $CD14^+$) were isolated using CD14-positive selection magnetic beads (cat. no. 130–050–201, Miltenyi Biotec). DCs were obtained by culture in the presence of 1000 IU/ml of granulocyte-macrophage colony-stimulating factor and interleukin-4 (cat. no. 215-GM-500 and Ref. 204-IL-500, R&D) for seven days and replacement of media and cytokines every two days. Activated DCs were differentiated by culturing immature DCs at day five for two more days in the presence of 100 ng/ml lipopolysaccharide (LPS, Ref. L4391–1MG Sigma-Aldrich). CD169 expression in mature DCs was detected by flow cytometry upon blocking with 1 mg/ml of human IgG (Privigen, Behring CSL) for 30 min at room temperature, followed by staining with anti-Siglec-1-PE 7–239 mAb (cat. no. 346004, BioLegend) at 4°C for 30 min. Mouse IgG1-PE (cat. no. 400112, BioLegend) was included as an isotype control for this staining. Samples were analyzed using FACSCalibur (BD Biosciences) with the CellQuest and FlowJo (v10.8.1) software applications to evaluate the data collected.

HIV-1 and $EBOV_{eGFP\text{-}VP40}$ uptake experiments were performed by pulsing 0.25E6 DCs with a constant number of viral particles per condition at 37°C for 4 hours. Cells were pre-incubated for 15 min at room temperature with 10 μg/ml of anti-CD169 mAbs or an IgG1 isotype control (BD Biosciences), or they were left untreated before exposure to virus. After extensive washing with PBS buffer, cells were acquired by flow cytometry (FACSCantoII, BD), and the frequency of positive cells was determined using FlowJo (v10.8.1 TreeStar). Forward-angle and side-scatter light gating were applied to exclude dead cells and debris from all analyses (Fig S1).

For HIV-1 *trans*-infection assays, 0.25E6 DCs were incubated with a constant amount of HIV-1_{NL4-3} for 4 h at 37ºC. Cells were pre-incubated for 15 min at room temperature with 10 μg/ml of anti-CD169 mAbs or an IgG1 isotype control (BD Biosciences) or were left untreated before viral exposure. After extensive washing, cells were co-cultured with the reporter cell line TZM-bl at a 1:1 ratio to measure *trans*-infection. Co-cultures were assayed for luciferase activity 48 hours later (BrightGlo luciferase system; Promega) using an EnSight Multimode Plate Reader (Perkin Elmer). Background values from non-HIV-1–pulsed co-cultures were subtracted for each experiment.

Fusion assays were performed as described previously [23]. When non-infectious $EBOV_{BlaM\text{-}VP40}$ VLPs fuse with cellular membranes, they release β-lactamase, which can then cleave a CCF2-AM dye loaded into the DC cytoplasm and change its fluorescence emission from fluorescein to coumarin. As opposed to the system previously used to detect viral uptake, this assay selectively detects Ebola VLPs entering the cytoplasm by fusion. DCs were preincubated or not with anti-CD169 mAbs (see above). A constant fusogenic amount of $EBOV_{BlaM\text{-}VP40}$ VLPs was added to 0.25E6 cells and incubated overnight at 37°C. To use equivalent numbers of fusogenic viral particles in all entry assays, $EBOV_{BlaM\text{-}VP40}$ VLP stocks were titrated in duplicate with serial 50% dilutions in Vero E6 cells (3E4per well) seeded in 96-well plates, loaded with CCF2-AM substrate, and analyzed using flow cytometry (FACSCantoII, BD). The CCF2-AM substrate (cat. no. K1032, Invitrogen) was added to cells following the manufacturer's instructions to identify cells in which $EBOV_{BlaM\text{-}VP40}$ VLP fusion had occurred. Cells were assessed using flow cytometry (FACSCantoII, BD), and the percentage of positive cells was determined with FlowJo software.

For SARS CoV-2 uptake experiments, the procedure followed was as described elsewhere [25]. 0.25E6 DCs were pulsed with a constant number of viral particles per condition at 37°C for 3 h. Cells were pre-incubated for 15 min at room temperature with 10 μg/ml of anti-CD169 mAbs or an IgG1 isotype control (BD Biosciences), or they were left untreated before viral exposure. After extensive washing with PBS buffer, SARS-CoV-2 nucleocapsid protein in the cells was quantified using highly sensitive quantitative ELISA (cat. no. 41A228R, BioVendor) to determine virus uptake.

According to a previously described method used for *trans*-infection experiments in SARS-CoV-2 [25], HEK-293 T over-expressing the human ACE2 or lacking this molecule were used to test whether replication-competent SARS-CoV-2 was *trans*-infected. Uptake experiments with SARS-CoV-2 were performed by pulsing 0.25E6 LPS-activated DCs with a multiplicity of infection of 0.75 for 3 hours at 37ºC. After extensive washing, cells were co-cultured at a ratio of 3:1

with HEK-293 T cells expressing ACE2 and TMPRSS2 receptors. Six days later, the supernatant was assayed using a SARS-CoV-2 nucleocapsid protein high-sensitivity quantitative ELISA (cat. no. 41A228R, BioVendor).

2.8. Induction of oxidative stress and SEC-MALS analysis

Oxidative stress to the antibodies investigated was induced by incubating them with 0.1% hydrogen peroxide solution for 20 min at 37°C and quenching with 80 mm Met aqueous solution as described elsewhere [20]. The resulting protein solution was analyzed using size-exclusion chromatography and multi-angle-light-scattering (SEC--MALS) to estimate the size distribution and relative aggregate formation. Thus, 0.050 mg of each antibody at 1 mg/ml was injected into a Superdex200 10/300 GL, id0026 column coupled to an Agilent 1260 infinity II HPLC system equipped with an SPD-20AS UV7VIS detector (Shimadzu), miniDAWN (Wyatt), Optilab (Wyatt) using PBS as a running buffer with flow set at 0.75 ml/min. Graphs were plotted using the UV signal. Further analyses were performed, and the molecular weight was calculated via multi-angle and dynamic light scattering using the Astra software (version 7) of Wyatt Technologies.

2.9. Surface plasmon resonance analysis

The binding curves were analyzed, and the affinity of the humanized mAb variants for CD169 was calculated using surface plasmon resonance on the IBIS MX96 platform (IBIS Technologies) with equilibrium analysis as described elsewhere [6,7]. In brief, anti-CD169 antibodies and controls were spotted on a single Easy2Spot G-type sensor (Ssens) at 60-nM, 20-nM, and 6-nM concentrations in 10 mM of sodium acetate buffer, pH4.5, using a continuous flow microspotter (Wasatch). The CD169 protein (cat. no. 5197-SL-050, R&D Systems) was injected over the sensor in 12 increasing concentrations ranging from 0.049 to 100 nM, thus enabling binding to be measured using surface plasmon resonance. Regeneration after each sample was carried out with 10 mM glycine-HCl, pH2.0. Association and dissociation were monitored to calculate dissociation constants (K_D) in Scrubber version 2 software (Biologic Software) and then interpolated to one specific Rmax = 1000 RU using Excel.

2.10. Retrogenix cell microarray

Custom pre-screens, full screens, and post-screens were carried out using Retrogenix as described previously [11]. Library screening was based on 6052 expression vectors encoding both ZsGreen1 and a full-length secreted human plasma membrane protein or a secreted cell surface–tethered human protein, plus a further 397 human heterodimers, which were individually arrayed in duplicate across cell microarray slides ('slide-sets'). Human HEK293 cells were transfected with an expression vector (pIRES-hEGFR-IRES-ZsGreen1) containing recombinant proteins. After cell fixation, h_1-3F1 mAb was added to each slide at 1 μg/ml, and binding was detected using the fluorescent secondary antibody as anti-hIgG-Fc-AF647. This was screened against two replicate slide-sets. Fluorescent images were analyzed and quantitated for transfection using ImageQuant software (GE Healthcare, Version 8.2). A protein 'hit' is defined as a duplicate spot showing a raised signal compared with background levels. This is achieved by visual inspection using the images gridded on the ImageQuant software. To confirm the hits and assess specificity, vectors encoding all hits identified during Library screening were arrayed and expressed in HEK293 cells on new slides. The slides were treated after cell fixation or in the absence of cell fixation with 1 μg/ml of h_1-3F1 mAb, 1 μg/ml of rituximab biosimilar (positive control), or no test molecule (secondary antibody only; negative control). Binding to target-expressing cells and untransfected cells was again assessed using fluorescence imaging.

For the flow cytometry validation study, human HEK293 cells were transfected with expression vectors encoding ZsGreen1 only, ZsGreen1-CD169, ZsGreen1-SUSD5, or ZsGreen1-CD20 (assay control). Live cell transfectants were incubated with 1 μg/ml of h_1-3F1 mAb, 1 μg/ml of rituximab biosimilar (assay control), or assay buffer only. Cells were washed and incubated with the same AF647 anti-hIgG Fc detection antibody as used in the cell microarray screens. Cells were again washed and analyzed using flow cytometry with an Accuri flow cytometer (BD). A 7AAD live/dead dye was used to exclude dead cells from the analysis, and ZsGreen-positive cells (transfected) were selected for analysis.

2.11. Statistical analysis

Mean changes in all the normalized data were evaluated to measure mAb blocking capacity. A one-sample Wilcoxon test was performed to determine significance, and p values of < 0.05 were considered significant. Data are presented as mean ± SD. The statistical analysis was performed with GraphPad Prism 9 for Windows (GraphPad Software).

3. Results

3.1. Humanization of anti-CD169-mAbs

From our previous study [23], we selected three anti-CD169 mAbs that had been generated in mice (clones #1F5, #3F1 and #5B10) based on their ability to recognize the CD169 cellular receptor and to block HIV-1 virus-like particle (VLP) uptake with the highest efficiency. After obtaining their genomic sequences from the corresponding hybridomas, we generated two humanized variants for the three candidates selected based on chimeric genetic recombination or complementarity-determining region (CDR)–engrafted technologies (Fig. 1**A**). To generate CDR-engrafted humanized antibodies (named h_0), mouse variable regions from heavy and light chains (VH and VL, respectively) of #1F5, #3F1, and #5B10 antibodies were aligned according to Ig Blast-NCBI to find the closest human related V gene and to identify the framework residues (FRs) and CDRs. During this process, mouse residues forming the CDRs were retained, while the FRs that did not match between the mouse and the human germlines were changed to the residue present in the human V gene. A summary of the closest human related V genes identified for each mAb and the respective identity to the human germline is reported in Table 1.

The six mAbs were cloned into the human IgG1 format, the most abundant IgG subclass in humans, which also retains good complement activity, Fc-receptor–mediated effector function, and a half-life of three weeks [5,7]. Chimeric and humanized CDR–engrafted antibodies were produced by transient transfection in HEK293FS cells and purified using Protein A. Based on their purity and integrity, as well as on SDS-PAGE and Western blot analysis under both reducing and non-reducing conditions, we confirmed that the antibodies produced were human IgG1/kappa.

To examine a functional consequence of this humanization processes, we analyzed whether these new antibodies maintained their ability to block viral binding of enveloped viruses to CD169. Thus, we performed a functional competition assay with Raji-Siglec-1 cells and HIV-1 VLPs, which expressed eGFP as a reporter gene, thus enabling the binding of viral particles to be quantified by flow cytometry. In this way, we were able to compare the effect of the newly generated antibodies targeting CD169 with the original murine mAbs, which serve as the corresponding positive blocking control (Fig. 1**B-D**). Additionally, we measured half maximal inhibitory concentration (IC_{50}) to facilitate comparison (Fig. 1**E**). As shown, there were no substantial differences in the IC_{50} during humanization of antibodies #1F5 and #3F1, since all IC_{50} values are less than 2 μg/ml and remain in the same range.

As a result of the successful CDR-grafted humanization of #1F5 and #3F1, we decided to discontinue further development of clone #5B10 and chimeric versions of the antibodies that, despite having lower IC_{50} values, could more readily elicit adverse responses when administered

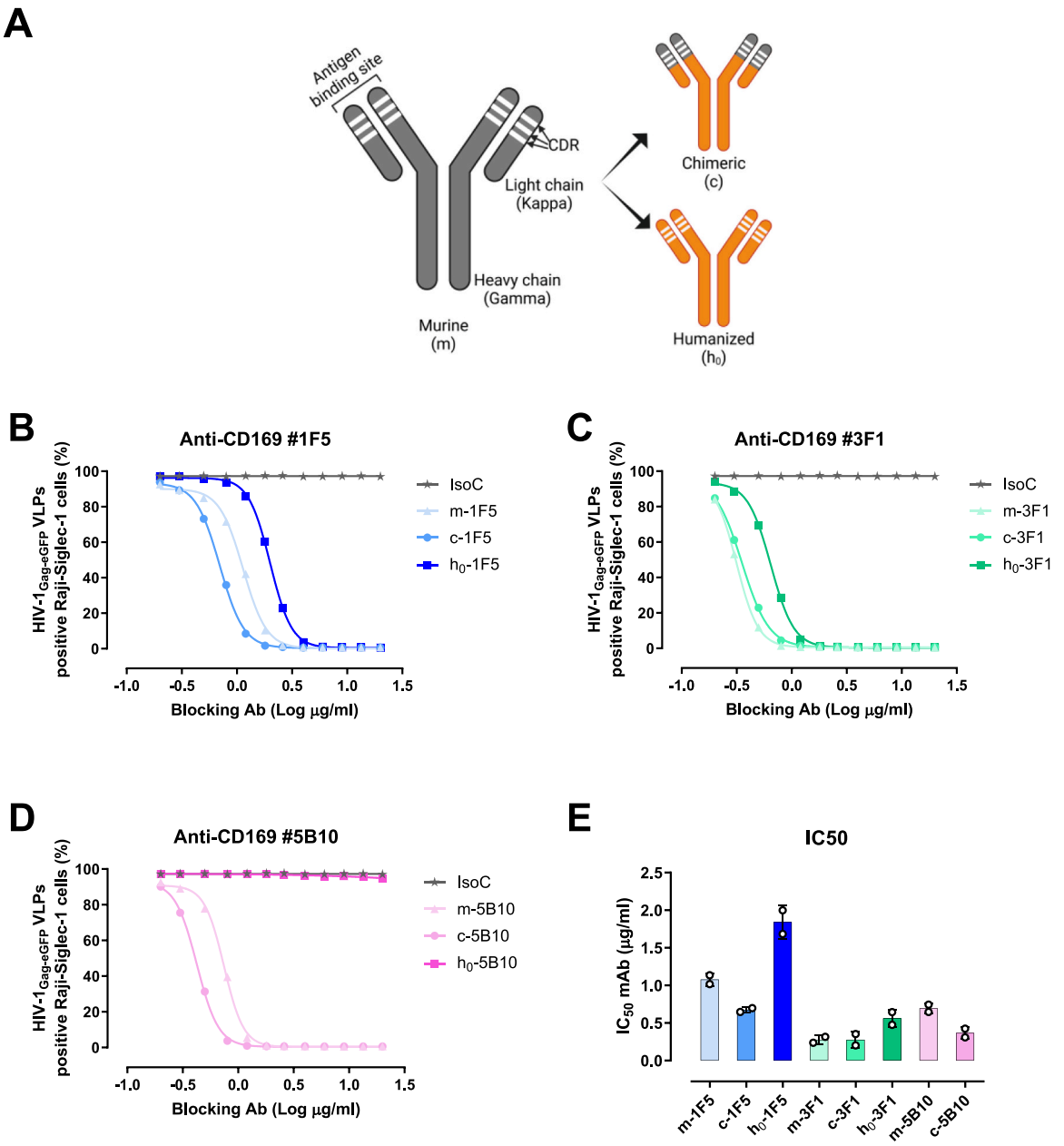

Fig. 1. Humanization of anti-CD169-mAbs and functional validation. **A.** Diagram illustrating the design of humanized anti-CD169 mAbs. Created with Biorender. **B. C. D.** Competition for Raji-Siglec-1 cells binding between HIV-$1_{Gag\text{-}eGFP}$ VLPs and 3 different anti-CD169 mAbs for 1 h at 37°C. The antibody isotype control was used as a reference (IsoC, with grey star symbols). A comparison between original murine antibody (m-, triangle and lighter color), chimeric antibody (c-, circle), and humanized CDR-engrafted antibody (h_0, square and darker color) is shown for each antibody clone (#1F5, **B**; #3F1, **C**; #5B10, **D** [corresponding to a non-linear fit to a variable response curve from one representative experiment out of two]). **E.** IC_{50} values of individual mAbs that achieved a total HIV-$1_{Gag\text{-}eGFP}$ VLP blocking effect. Data from two independent experiments.

in patients.

3.2. Optimization of humanized anti-CD169-mAbs

We experimentally evaluated the effect of potential instabilities to optimize the selected anti-CD169 mAb and thus anticipate limitations that could occur during formulation, manufacturing, and storage. Hence, we further improved the humanized CDR-grafted monoclonal antibodies #1F5 and #3F1 by removing potential sequencing liabilities in the initial phase of the antibody engineering process. We used the SAbPred structure-based antibody prediction server for this investigation [8]. The potential sequence liabilities detected are summarized in Table 2.

Subsequently, each liability identified was evaluated by searching scientific publications for potential hotspots that have already been shown to have a negative impact during the biological medicine manufacturing process. For each liability identified, we further assessed whether these residues form part of CDRs or FRs. The potential liabilities present in human FRs were retained except for one. These conserved regions are less susceptible to chemical instability because they are buried within the 3D protein structure and are therefore less accessible to solvents. However, since they could play an important role in the correct folding of antibodies, we focused our evaluation by introducing mutations at potential hotspots mapped to the CDRs owing to their relative flexible and solvent accessibility (Fig. 2**A**).

Analysis of the h_0-1F5 antibody revealed the presence of a

Table 1
Sequence alignment of CDR regions from original murine and humanized anti-CD169 antibodies to the closest human gene.

			Identity	CDR1												CDR2								CDR3												
#1F5	VH	IGVH 1–2*06		G	Y	T	F	T	G	Y	Y					I	N	P	N	S	G	G	T	A	R										D	Y
		Mouse (m)	63/98 matches	-	-	-	-	-	D	-	F					-	Y	-	G	-	-	H	I	-	-	Y	S	T	L	D	Y	Y	V	M	-	Q
		Humanized (h_0)	91/98 matches	-	-	-	-	-	D	-	F					-	Y	-	G	-	-	H	I	-	-	Y	S	T	L	D	Y	Y	V	M	-	Q
	VL	IGKV4–1*01		Q	S	V	L	Y	S	S	N	N	K	N	Y	W	A	S						Q	Q					Y	T					
		Mouse (m)	76/99 matches	-	T	L	F	N	-	G	T	R	-	-	-	-	-	-						K-	-	S	Y	N	L	L	-					
		Humanized (h_0)	90/99 matches	-	T	L	F	N	-	G	T	R	-	-	-	-	-	-						K	-	S	Y	N	L	L	-					
#3F1	VH	IGHV 1–3*01		G	Y	T	F	T	G	Y	Y					I	N	P	N	S	G	G				A	R									
		Mouse (m)	65/98 matches	-	-	S	-	-	T	-	-					-	S	C	Y	N	-	A		A	R	K	G	G	W	I	P	F				
		Humanized (h_0)	91/98 matches	-	-	S	-	-	T	-	-					-	S	C	Y	N	-	A		A	R	K	G	G	W	I	P	F				
	VL	IGKV4–1*01		Q	S	V	L	Y	S	S	N	N	K	N	Y	W	A	S							Q	Q										
		Mouse (m)	80/100 matches	-	-	-	-	N	-	-	-	Q	-	-	F	-	-	-						H	-	Y	L	S	S							
		Humanized (h_0)	94/100 matches	-	-	-	-	N	-	-	-	Q	-	-	F	-	-	-						H	-	Y	L	S	S							
#5B10	VH	IGHV 1–46*01		G	Y	TF	F	T	G	Y	Y					I	N	P	N	S	G	G	T												D	V
		Mouse (m)	63/98 matches	-	-	-	-	S	T	-	W					-	A	-	S	D	-	Y	-	G	G	F	Y	D	G	Y	P	D	F	F	-	F
		Humanized (h_0)	92/98 matches	-	-	-	-	S	T	-	W					-	A	-	S	D	-	Y	-	G	G	F	Y	D	G	Y	P	D	F	F	-	F
	VL	IGKV4–1*01		Q	S	V	L	Y	S	S	N	N	K	N	Y	W	A	S						Q	Q						Y	T				
		Mouse (m)	76/101 matches	-	-	L	-	N	-	N	T	Q	R	-	-	F	-	-						-	-	H	Y	S	S	P	-	-				
		Humanized (h_0)	92/101 matches	-	-	L	-	N	-	N	T	Q	R	-	-	F	-	-						-	-	H	Y	S	S	P	-	-				

Table 2
Potential sequence liabilities in humanized 1F5 and 3F1 anti-CD169 antibodies.

		Aa in h_0	Region	Risk	Suggested Aa in h_1
#1F5	VH	M34	FR2H	Oxidation	
		M70	FR3H	Oxidation	
		S76	FR3H	Immunogenicity	I76
		M107	CDR3H	Oxidation	L107
		W110	FR4H	Oxidation	
	VL	M4	FR1L	Oxidation	
		N31;S32	CDR1L	Deamidation	
		W41	FR1L	Oxidation	
		W56	CDR2L	Oxidation	F56
#3F1	VH	M34	FR2H	Oxidation	
		W50	FR2H	Oxidation	
		C53	CDR2H	Folding	A53
		N55;G56	CDR2H	Deamidation	S55; G56
		W102	CDR3H	Oxidation	F102
		W108	FR4H	Oxidation	
	VL	M4	FR1L	Oxidation	
		N31;S32	CDR1L	Deamidation	S31; S32
		N31	CDR1L	Stability	S31
		S32	CDR1L	Stability	
		S33	CDR1L	Stability	
		W41	FR2L	Oxidation	
		W56	CDR2L	Oxidation	F56

methionine in the CDR3 of the heavy chain and a tryptophan in the CDR2 of the light chain, entailing a risk of oxidation that can negatively affect antigen binding at the CD169 receptor. We replaced these residues with a leucine and phenylalanine, respectively. Furthermore, S76 in FR3 of the heavy chain was replaced by an isoleucine because it is normally found in the closest human VH germline sequences.

Analysis of the h_0-3F1 antibody showed that the CDR2 in the heavy chain contains an unpaired cysteine that can cause folding and aggregation problems; therefore, it was replaced by an alanine. It also revealed a motif at risk of deamidation (N55-G56) in the same region that was exchanged for S55-G56. Moreover, a tryptophan with risk of oxidation in the CDR3 of the heavy chain was replaced by the more stable phenylalanine. In the light chain, an N-linked glycosylation site present in CDR1 exerts a modification effect that can only be determined experimentally given the controversial results reported for Fab glycans. This same residue is also included in a deamidation risk motif (N31; S32); therefore, we removed both liabilities by replacing asparagine 31 by a serine, a non-glycosylated residue. In addition, tryptophan at position 56 of the light chain was considered a potential oxidation target and was therefore replaced by phenylaniline.

To test whether these modifications alter the viral binding and blocking capabilities of humanized antibodies, we generated five variants of the h_0-1F5 antibody and eight variants of the h_0-3F1 antibody by combining the stabilizing mutations described above (Fig. 2**A**). We then performed a competition assay between HIV-$1_{Gag\text{-}eGFP}$ VLPs and those anti-CD169 mAb variants at a single concentration, which completely blocks the uptake of HIV-$1_{Gag\text{-}eGFP}$ by h_0-1F5 and h_0-3F1 (Fig. 2**B**). All mutations introduced in the h_0-1F5 antibody lose the ability to block viral uptake, except variant 4, with exchange of S76I residue in the light chain. On the other hand, the mutations introduced in the h_0-3F1 antibody lose the ability to block viral uptake, except for variant 6, which lost the unpaired cysteine C53 and the deamination motif in the heavy chain.

These two mAb variants with blocking activity similar to that of the parental antibody (now designated h_1-1F5 and h_1-3F1) were selected as lead candidates and investigated further. First, we performed the same functional competition assay with Raji-Siglec-1 cells and HIV-$1_{Gag\text{-}eGFP}$-VLPs at increasing concentrations of antibody (Fig. 2**C**) to determine the corresponding IC_{50} (Fig. 2**D**). Thus, mAb h_1-3F1 maintains a blocking capacity similar to that of the parental antibodies, while h_1-1F5 showed a higher IC_{50}, similar to h_0-1F5.

A

Variant	V_H: S76I	V_H: M107L	V_L: W56F
h_0-1F5	S76	M107	W56
Var1	I76	L107	F56
Var2	I76	M107	F56
Var3	I76	L107	W56
Var4	I76	M107	W56
Var5	S76	M107	F56

Variant	V_H: C53A	V_H: N55S	V_H: W102F	V_L: N31S	V_L: W56F
h_0-3F1	C53	N55	W102	N31	W56
Var1	A53	S55	F102	S31	F56
Var2	A53	S55	W102	S31	F56
Var3	A53	S55	F102	S31	W56
Var4	A53	S55	W102	S31	W56
Var5	A53	S55	F102	N31	W56
Var6	A53	S55	W102	N31	W56
Var7	C53	N55	W102	S31	F56
Var8	C53	N55	W102	S31	W56

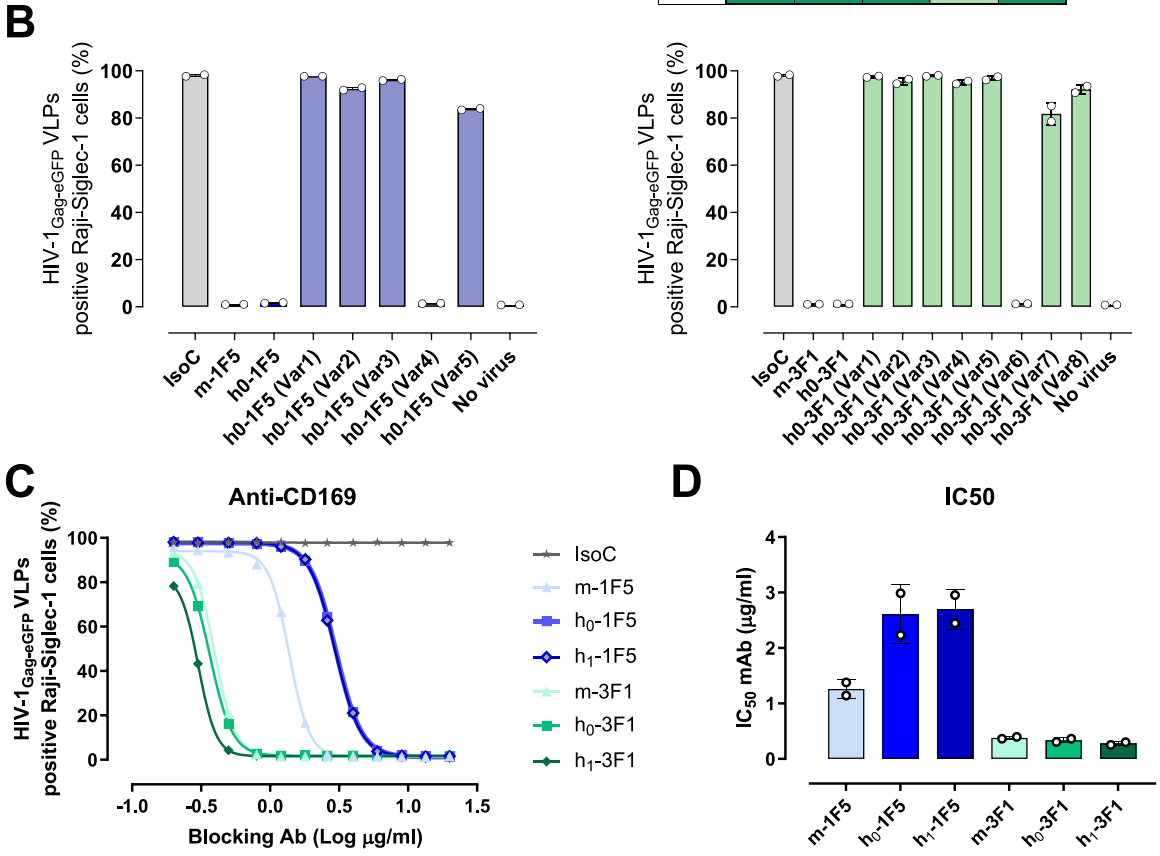

Fig. 2. Optimization of humanized anti-CD169 mAbs and functional validation. **A.** Potential sequence liabilities found in CDR-engrafted humanized antibodies define variants indicated by suggested amino acid exchanges. **B.** Competition assay with Raji-Siglec-1 cell binding and HIV-$1_{Gag\text{-}eGFP}$ VLPs to test anti-CD169 mAb variants to eliminate selected potential liabilities. **C.** Competition for Raji-Siglec-1 cell binding between HIV-$1_{Gag\text{-}eGFP}$ VLPs and anti-CD169 mAbs. We tested the three different forms of #1F5 and #3F1 antibodies: murine (m-, triangle and lighter color), humanized (h_0-, square), and stabilized (h_1-, diamond). The comparison between these antibodies is shown with a non-linear fit to a variable response curve from one representative experiment out of two. **D.** IC_{50} values of individual mAbs were calculated with a non-linear fit to a variable response curve. Data from two independent experiments.

3.3. *Humanized anti-CD169 mAbs block viral entry into primary DCs*

We next evaluated whether humanized anti-CD169 mAbs could block HIV-1 uptake and *trans*-infection. For this, we used LPS-activated monocyte-derived DCs as previously reported [14,23,27]. We used fluorescent HIV-$1_{NL4\text{–}3\ Gag\text{-}iGFP}$, which is as infectious as native HIV-1 [13]. LPS-activated DCs were pre-incubated with anti-CD169 mAbs or an isotype control antibody before adding a constant amount of HIV-$1_{NL4\text{–}3\ Gag\text{-}iGFP}$. Pre-treatment with humanized anti-CD169 mAbs inhibited viral capture, as did murine anti-CD169 mAbs (Fig. 3**A**). We also tested the ability of humanized anti-CD169 mAbs to block HIV-1 *trans*-infection. To do so, we used the infectious replicative virus HIV-$1_{NL4\text{–}3}$. LPS-activated DCs were pre-incubated with anti-CD169 or isotype control mAbs and pulsed with equivalent amounts of HIV-$1_{NL4\text{–}3}$. After extensive washing, the DCs were co-cultured with the TZM-bl $CD4^+$ reporter cell line to measure luciferase production upon transfer of HIV-$1_{NL4\text{–}3}$ particles to these cells (Fig. 3**B**). As previously observed for viral uptake, humanized anti-CD169 mAbs efficiently blocked HIV-1 *trans*-infection.

To evaluate the ability of humanized anti-CD169 mAbs to block EBOV uptake into primary DCs, we used fluorescent Ebola VLPs containing EBOV structural proteins fused to eGFP (EBO$V_{eGFP\text{-}VP40}$ VLPs). LPS-activated DCs were pre-incubated with anti-CD169 mAbs or an isotype control before adding a constant amount of EBO$V_{eGFP\text{-}VP40}$ VLPs. Pre-treatment with humanized anti-CD169 mAbs inhibited DC capture, as did murine anti-CD169 mAbs (Fig. 3**C**). We also tested whether novel anti-CD169 mAbs could affect cytoplasmic viral fusion in LPS-activated DCs. Thus, we used Ebola VLPs containing the BlaM-VP40 chimeric protein and the viral glycoprotein and nucleoprotein (EBO$V_{BlaM\text{-}VP40}$ VLPs). LPS-treated DCs were pre-incubated with anti-CD169 mAbs or isotype control and pulsed with equivalent amounts of EBPV$_{BlaM\text{-}VP40}$ VLPs. After extensive washing, viral fusion was measured using flow cytometry (Fig. 3**D**). As previously observed for viral uptake, humanized anti-CD169 mAbs efficiently blocked Ebola VLP fusion and release of

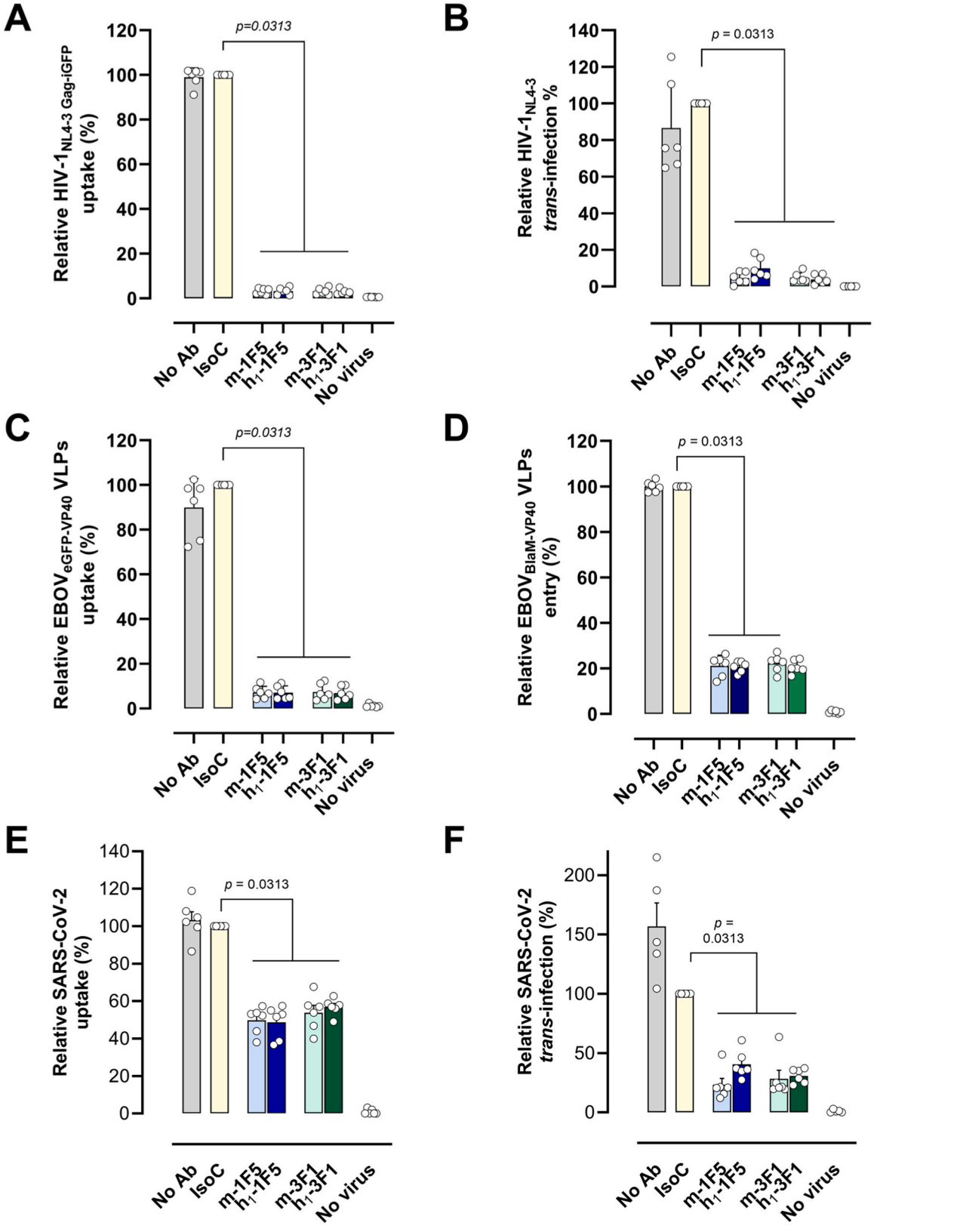

(caption on next page)

Fig. 3. Humanized anti-CD169 mAbs block DC-mediated viral entry. **A.** Relative viral uptake of HIV-1 by LPS-activated DCs. Cells were pre-incubated with humanized anti-CD169 mAbs and then pulsed for 4 h at 37ºC with non-replicative HIV-$1_{NL4-3\ Gag\text{-}iGFP}$. Values are normalized to cells incubated with isotype control mAb, showing a mean ± SD entry of 78.8 ± 9.7%, which is considered 100%. **B.** Relative HIV-1_{NL4-3} *trans*-infection mediated by LPS-treated DCs pre-incubated with anti-CD169 mAbs. Values are normalized to cells pre-incubated with isotype control mAb, showing a mean ± SD entry of 2.83 ×106 RLU ± 2.3 ×106, which is considered 100%. **C.** Relative viral uptake of $EBOV_{eGFP\text{-}VP40}$ VLPs by LPS-activated DCs. Cells were pre-incubated with humanized anti-CD169 mAbs and then pulsed for 4 h at 37ºC. Values are normalized to uptake by cells incubated with isotype control mAb, with a mean ± SD entry of 51.2 ± 18.7%, which is considered 100%. **D.** Relative internalization of $EBOV_{BlaM\text{-}VP40}$ VLPs by LPS-activated DCs pre-incubated with anti-CD169 mAbs. Values are normalized to cells incubated with isotype control mAb, with a mean ± SD entry of 46.8 ± 14.2%, which is considered 100%. **E.** Relative viral uptake of SARS-CoV-2 by LPS-activated DCs. Cells were pre-incubated with humanized anti-CD169 mAbs and then pulsed for 3 h at 37ºC. Values are normalized to cells incubated with isotype control mAb, with a mean ± SD entry of 13.65 ± 8.2 ng/ml, which is considered 100%. **F.** Relative SARS-CoV-2 *trans*-infection mediated by LPS-activated DCs pre-incubated with anti-CD169 mAbs. Values are normalized to cells incubated with isotype control mAb, with a mean ± SD entry of 12.3 ± 2.9 ng/ml, which is considered 100%. Data information: In (A–F), data are presented as mean values and SD from two independent experiments and include cells from six donors. Statistical differences were assessed using a one-sample Wilcoxon test.

reporter into the cytoplasm.

Finally, we assessed whether humanized anti-CD169 mAbs could block viral uptake and *trans*-infection of SARS-CoV-2. To block viral uptake, LPS-activated DCs were pre-incubated with anti-CD169 mAbs or an isotype control before adding a constant amount of SARS-CoV-2. Pre-treatment with humanized anti-CD169 mAbs inhibited DC capture, as did murine anti-CD169 mAbs (Fig. 3**E**). To evaluate SARS-CoV-2 *trans*-infection, LPS-treated DCs were pre-incubated with anti-CD169 mAbs or isotype control and pulsed with equivalent amounts of SARS-CoV-2 (see above). After extensive washing, DCs were co-cultured with HEK-293 T cells overexpressing the ACE2 receptor and the transmembrane protease TMPRSS2, which is required for SARS-CoV-2 infection, and viral nucleocapsid levels were measured in the culture supernatants to assess *trans*-infection (Fig. 3**F**). Once again, humanized anti-CD169 mAbs efficiently blocked SARS-CoV-2 *trans*-infection.

Taken together, these results show that humanization and optimization processes maintained functional recognition of CD169 to prevent binding of this cellular attachment receptor to gangliosides on viral envelope membranes, thus limiting virus spread.

3.4. Biochemical stability and affinity of humanized anti-CD169-mAbs

The data shown in Figs. 2 and 3 demonstrate the generation of two new stabilized variants of the humanized anti-CD169 antibodies #1F5 and #3F1, which exhibit the same functional activity as the non-stabilized parental antibody. We then further analyzed these antibodies under oxidative stress by evaluating their propensity for aggregation and their binding affinities.

Antibodies that underwent oxidative stress induced by hydrogen peroxide were characterized by SEC-MALS to determine the size distribution of the resulting protein solution (Fig. 4**A**). No aggregation or degradation products were detected after inducing oxidative stress, and the antibodies were pure and showed a monomeric peak. We performed the functional competition assay again with Raji-Siglec-1 cells and HIV-$1_{Gag\text{-}eGFP}$ VLPs at increasing concentrations of antibody to assess whether the stabilized humanized anti-CD169 mAbs maintain their blocking capacity under oxidative stress (Fig. 4**B**). As illustrated, while h_1-1F5 and the parental h_0-1F5 completely lose their blocking capacity after hydrogen peroxide treatment, the mAb h_1-3F1 maintains the blocking capacity of the parental antibodies, even after oxidative stress.

We then analyzed the binding affinity of these treated antibodies for their primary target, the CD169 receptor, using surface plasmon resonance (Fig. 4**C**). Affinity measurements were similar when humanized and stabilized variants were compared after oxidative stress. Interestingly, both h_0-1F5 and stabilized h_1-1F5 bound weakly to the CD169 target, and the dissociation constants (K_D) could not be determined (Fig S2). This correlates with an increase in the IC_{50} calculated after the humanization process (Figs. 1**E** and 2**D**). On the other hand, both h_0-3F1 and stabilized h_1-3F1 bound equally well to the CD169 target, and the calculated K_D ranged between 3.8E-8 M and 5.4E-8 M, correlating with a lower and conserved IC_{50} after humanization and stabilization (Fig. 2**D**).

In view of these results, we used Retrogenix Cell Microarray Technology to detect specific off-target binding interactions of the mAb h_1-3F1. This methodology tested our antibody at 1 μg/ml against 6052 full-length human cell membrane proteins and 397 human heterodimers, revealing a total of 58 library hits that were re-expressed and re-tested in both fixed and live cells. As expected, the h_1-3F1 antibody underwent a specific interaction with CD169, its primary target. An additional specific interaction with the SUSD5 protein was observed in live and fixed cell microarrays. When these interactions were further investigated using flow cytometry at a single antibody concentration, we observed strong fluorescence intensity binding to CD169 and medium/strong fluorescence intensity binding to SUSD5 (Fig. 4**E**). These data indicate that h_1-3F1 binds specifically to its primary target and undergoes a secondary interaction with SUSD5. The very limited existing information about SUSD5 would require additional dose-response flow cytometry studies and functional assays to determine its biological relevance. In conclusion, of more than 6400 proteins analyzed, only one additional interaction was observed with SUSD5, albeit with lower affinity than for CD169. This highlights the powerful applicability of our antibody for preventing CD169 binding as a therapeutic strategy.

4. Discussion

Monoclonal antibodies have revolutionized outcomes in cancer, autoimmune diseases, and other conditions, making them an essential component of current treatments. From a product development standpoint, engineered chimeric and humanized mAbs are considered optimal, as they are generally associated with a lower risk of immunogenicity and may have longer circulating half-lives than their murine counterparts [9]. With the aim of carrying out future clinical studies, we humanized and stabilized 3 murine anti-CD169 mAbs clones with broad antiviral activity. The therapeutic mechanism is based on the specific interaction of the anti-CD169 mAb with the CD169 expressed on the surface of DCs, thus preventing binding of CD169 to the sialylated gangliosides present on the viral envelopes and inhibiting viral uptake [15,23,25,27]. Therefore, after determining the genomic sequence of these clones (designated #1F5, #3F1 and #5B10) to identify the mouse residues that form the CDRs, we generated mAb variants on a human IgG1 scaffold. Depending on the application, IgG1 can also be further engineered to extend the half-life and avoid interaction with complement and/or Fc-receptor–mediated effector functions.

Although IgG antibodies are relatively stable molecules, they are subject to a variety of degradation reactions that can occur during formulation, manufacturing, and storage. Post-translational modifications have the potential to reduce the affinity/potency, stability, and homogeneity of an antibody, resulting in complications in downstream processes [19]. The VH and VL antibody sequences contain multiple motifs subject to chemical instability that can affect antigen binding, such as oxidation, glycosylation, deamidation, and isomerization in the antibody CDR sequences. Oxidation is a common chemical degradation pathway of protein therapeutics. It can be induced by exposure to light, thermal stress, or impurities such as metal ions and peroxides. Although

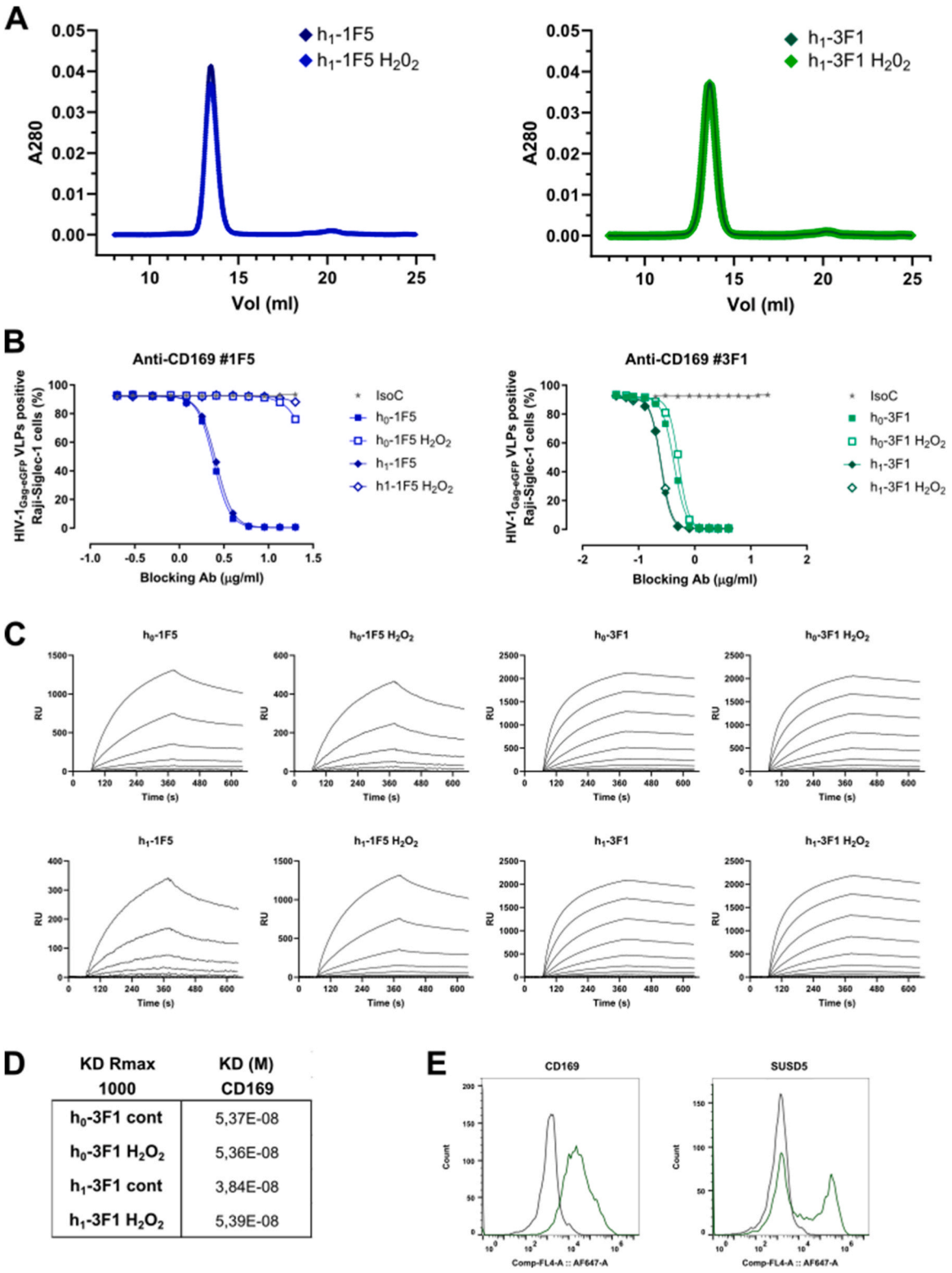

KD Rmax 1000	KD (M) CD169
h_0-3F1 cont	5,37E-08
h_0-3F1 H_2O_2	5,36E-08
h_1-3F1 cont	3,84E-08
h_1-3F1 H_2O_2	5,39E-08

Fig. 4. Stability and affinity analysis of humanized and stabilized anti-CD169-mAbs under oxidative stress. **A**. Chromatogram of anti-CD169-mAbs before and after H_2O_2-induced oxidative stress measured by SEC-MALS. **B**. Competition for Raji-Siglec-1 cell binding between HIV-$1_{Gag\text{-}eGFP}$ VLPs and anti-CD169 mAbs. We tested two different forms of #1F5 and #3F1 antibodies, namely, humanized (h_0-, square) and stabilized (h_1-, diamond), before (filled symbols) and after (empty symbols) treatment with H_2O_2-induced oxidative stress. Non-linear fit to a variable response curve from one representative experiment out of two. **C**. Sensograms of anti-CD169 mAbs coupled on SPR sensor arrays at 60 nM show binding to their target CD169 receptor in solution using the IBIS MX96 platform before and after oxidative stress. The response scale (Y-axis) is adjusted to show on and off rates for all antibodies, as sensor coupling seemed to be affected by amino acid changes introduced in #1F5 mAb, compared to #3F1 mAb, which showed similar coupling efficiencies upon optimization. The graphs show that on- and off-rates for both antibodies are unaffected by amino acid exchange and oxidative stress. **D**. Calculation of K_D by interpolation of equilibrium fit for #3F1 mAb from Fig. 4C. CD169 binding to #1F5mAb was too weak to calculate K_D. **E**. Flow cytometry profiles show the level of binding of h_1-3F1 at 1 µg/ml to HEK293 cells transiently transfected with ZsGreen1-CD169 or ZsGreen1-SUSD5 recombinant proteins. Antibody binding using a secondary antibody labelled with the fluorophore AF647.

methionine is the residue most susceptible to oxidation in mAbs, this oxidation has been reported in other residues such as tryptophan, cysteine, tyrosine, and histidine. Tryptophan residues are commonly found in CDRs owing to their structural features and hydrophobic properties, which confer common recognition sites that facilitate strong and specific binding between mAbs and their respective antigens [12]. Other common chemical modifications of interest for mAbs are deamidation and isomerization. Deamidation of asparagine residues and isomerization of aspartate in biological pharmaceuticals is a major cause of degradation if pharmaceutical proteins are not properly formulated and stored. These chemical mechanisms are pH- and temperature-dependent and involve several competing transition states [18]. Furthermore, IgGs can contain N-linked glycans in the variable domains, the so-called Fab glycans, in addition to the Fc glycans. These Fab glycans are acquired after the introduction of N-glycosylation sites during somatic hypermutation and thereby constitute part of the physiological repertoire of antibodies. Furthermore, Fab glycans are often located near antigen-binding sites, can influence antigen binding, and contribute to affinity maturation. Conversely, some groups have reported that glycans in variable domains improve antibody solubility and stability, while recent literature indicates that Fab glycans can trigger aggregation [3]. These liability risks must be controlled during formulation or eliminated by replacing chemically unstable amino acid residues. However, only a subset of these motifs produces actual chemical modification; others almost always occur and may even be necessary for antigen binding. Therefore, amino acid exchange needs to be evaluated carefully. The modifications to and analyses of first-generation humanized (h_0) mAbs (Fig. 1) formed the basis for developing optimized anti-CD169 (h_1) mAbs that retain blocking activity against viral uptake and could therefore disrupt subsequent viral dissemination and cell-to-cell transfer during early infection (Fig. 3).

Enveloped viruses such as HIV-1, EBOV, and SARS-CoV-2 incorporate sialic acid–containing gangliosides on their viral envelope when they bud from cell membranes. These sialylated gangliosides are selectively recognized by the CD169 receptor, which is preferentially expressed on the surface of activated DCs, macrophages, and monocytes [26]. CD169 has been postulated as a molecular target for blockade of binding of enveloped viruses to this attachment receptor, which is present on myeloid cells, and early reduction of their systemic dissemination to distant tissues [24,26,29]. The rationale behind the development of anti-CD169 mAbs is supported by published work demonstrating that anti-CD169 antibodies can reduce HIV-1 and SARS-CoV-2 *trans*-infection *in vitro* [15,17,23,25,30]. Most antibodies developed as antiviral treatments to date target viral proteins with the aim of neutralizing viral activity, which depends on the specific recognition of a viral protein. Since our mAbs target a host protein exploited by a variety of viruses, CD169 may be a feasible therapeutic target against enveloped viruses, and anti-CD169 mAbs could represent a broad-spectrum antiviral therapy that can prevent the emergence of drug-resistant viral strains, unlike therapies targeting viral proteins [2].

The findings of this study are subject to a series of limitations. All experiments were performed *in vitro*; therefore, the immunogenicity of these humanized antibodies needs to be evaluated in animal models to monitor anti-mAb response dynamics and its relationship to therapeutic outcomes. Since the mAbs do not bind murine CD169, humanized mouse models with sufficient engraftment of myeloid cells would be required to ensure expression of the human CD169 protein and assess the actual binding through epitope recognition for this kind of study. Moreover, one could consider incorporating additional features previously described for IgG1 immunoglobulins to minimize potential off-target effects and extend the half-life of the mAbs.

Although treatments targeting HIV-1 infection are efficient [1,31] and vaccination has proven to prevent the more virulent effects of SARS-CoV-2 [10], treatment options in EBOV are limited. Since the CD169 receptor interacts with ganglioside on the viral envelope, an antiviral treatment targeting CD169, alone or in combination, could be extended to treat other infectious diseases caused by ganglioside-containing enveloped agents that may not have any effective treatment at this time. This could be an advantage when fighting early-stage infection or even as a protective measure, with the knowledge that the therapeutic blockade of this receptor should not cause serious side effects, since the existence of null individuals indicates that the receptor can be safely inhibited [21].

Funding sources

PR-I was supported by grant 2017 BP 00121 from the Catalan Agency of Management of University and Research Grants.

XM-T was supported by the Spanish Ministry of Science, Innovation and Universities and the European Regional Development Fund under agreement No. BES-2017–082900.

Research at the laboratory of JM-P is supported by the Spanish Ministry of Science, Innovation and Universities (grants PID2022–139271OB-I00, PID2019–109870RB-I00 and CB21/13/00063) and in part by Grifols. His laboratory has been funded by the NIH/NIAID (1 UM1 AI164561–01 and 1P01AI178376–01), EU HORIZON-HLTH-2021-DISEASE-04–07 (grants 101057100 and 101095606, European Union), Fundació La Marató de TV3 (grant 202130–30–31–32, Spain), and Generalitat de Valencia (grant PROMETEO/2021/036, Spain).

NI-U is supported by the Spanish Ministry of Science and Innovation (grant PID2020–117145RB-I00), EU HORIZON-HLTH-2021-CORONA-01 (grant 101046118), and by institutional funding from Pharma Mar and HIPRA.

CRediT authorship contribution statement

Federica Linty: Writing – review & editing, Methodology, Investigation, Formal analysis. **Xabier Muñiz-Trabudua:** Writing – review & editing, Investigation. **Itziar Erkizia:** Writing – review & editing, Methodology, Investigation, Formal analysis. **Javier Martinez-Picado:** Writing – review & editing, Validation, Supervision, Resources, Methodology, Investigation, Funding acquisition, Formal analysis, Conceptualization. **Patricia Resa-Infante:** Writing – review & editing, Writing – original draft, Visualization, Validation, Supervision, Project administration, Methodology, Investigation, Formal analysis, Data curation, Conceptualization. **Dàlia Raïch-Regué:** Writing – review & editing, Investigation. **Jordana Muñoz-Basagoiti:** Writing – review & editing, Investigation. **Daniel Perez-Zsolt:** Writing – review & editing, Investigation, Conceptualization. **Arthur E.H. Bentlage:** Writing – review & editing, Investigation. **Gestur Vidarsson:** Writing – review & editing, Resources, Methodology, Conceptualization. **Theo Rispens:** Writing – review & editing, Methodology. **Nuria Izquierdo-Useros:** Writing – review & editing, Conceptualization.

Declaration of Competing Interest

The authors declare the following financial interests/personal relationships which may be considered as potential competing interests: J. Martinez-Picado reports financial support from the Spanish Ministry of Science, Innovation and Universities (grants PID2022–139271OB-I00 and CB21/13/00063) and in part by Grifols. His laboratory has been funded by the NIH/NIAID (1 UM1 AI164561–01 and 1P01AI178376–01), EU HORIZON-HLTH-2021-DISEASE-04–07 (grants 101057100 and 101095606, European Union), Fundació La Marató de TV3 (grant 202130–30–31–32, Spain), and Generalitat de Valencia (grant PROMETEO/2021/036, Spain). He has also received institutional grants and educational/consultancy fees from AbiVax, AstraZeneca, Gilead Sciences, Grifols, Janssen, Merck Sharp & Dohme, and ViiV Healthcare, all outside the submitted work. P. Resa-Infante reports financial support from the Government of Catalonia Agency for Administration of University and Research Grants. N. Izquierdo-Useros

reports financial support from the Spain Ministry of Science and Innovation and Universities (grant PID2020–117145RB-I00 and 10.13039/501100011033, Spain) and EU HORIZON-HLTH-2021CORONA-01 (grant 101046118, European Union). She also has received institutional funding from Pharma Mar, Grifols, HIPRA, and Amassence, all outside the submitted work. A patent application based on this work has been filed with the European Patent Office (Application form no.: EP23382072) that include P. Resa-Infante, I. Erkizia, N. Izquierdo-Useros and J. Martinez-Picado as inventors.The remaining authors declare that they have no known competing financial interests or personal relationships that could affect the work reported in this paper.

Acknowledgements

We are grateful to J. Díaz from the CMCiB for his constant help at the BSL3 facility. We thank Ninotska Derksen for assisting with the HP-SEC experiments. The authors also acknowledge the crowdfunding initiative #Yomecorono (https://www.yomecorono.com) and Foundation Dormeur for financial support to acquire the QuantStudio-5 real-time PCR system and an Eclipse Ts2RFL inverted research microscope. Some figures were created with BioRender.com.

Disclosure and competing interest statements

A patent application based on this work has been filed (Application form no.: EP23382072).

The authors declare no financial or commercial conflicts of interest. J.M.-P. has received other institutional grants and educational/consultancy fees from AbiVax, AstraZeneca, Gilead Sciences, Grifols, Janssen, Merck Sharp & Dohme, and ViiV Healthcare, all outside the submitted work.

Appendix A. Supporting information

Supplementary data associated with this article can be found in the online version at doi:10.1016/j.biopha.2024.116726.

References

[1] M.G. Atta, S. de Seigneux, G.M. Lucas, Clinical pharmacology in HIV therapy, Clin. J. Am. Soc. Nephrol. 14 (2019) 435–444, https://doi.org/10.2215/CJN.02240218.

[2] R. Badia, E. Garcia-Vidal, E. Ballana, Viral-Host Dependency Factors as Therapeutic Targets to Overcome Antiviral Drug-Resistance: A Focus on Innate Immune Modulation, Front. Virol. 2 (2022) 935933, https://doi.org/10.3389/FVIRO.2022.935933.

[3] F.S. van de Bovenkamp, N.I.L. Derksen, M.J. van Breemen, S.W. de Taeye, P. Ooijevaar-de Heer, R.W. Sanders, T. Rispens, Variable Domain N-Linked Glycans Acquired During Antigen-Specific Immune Responses Can Contribute to Immunoglobulin G Antibody Stability, Front Immunol. 9 (2018), https://doi.org/10.3389/FIMMU.2018.00740.

[4] D. Chelius, D.S. Render, P.V. Bondarenko, Identification and characterization of deamidation sites in the conserved regions of human immunoglobulin gamma antibodies, Anal. Chem. 77 (2005) 6004–6011, https://doi.org/10.1021/AC050672D.

[5] T. Damelang, S.W. de Taeye, R. Rentenaar, K. Roya-Kouchaki, E. de Boer, N.I. L. Derksen, K. van Kessel, S. Lissenberg-Thunnissen, S.H.M. Rooijakkers, I. Jongerius, et al., The Influence of Human IgG Subclass and Allotype on Complement Activation, Immunol 211 (11) (2023) 1725–1735, https://doi.org/10.4049/jimmunol.2300307.

[6] G. Dekkers, A.E.H. Bentlage, T. Stegmann, H.L. Howie, S. Lissenberg-Thunnissen, J. James Zimring, T. Rispens, G. Vidarsson, Affinity of human IgG subclasses to mouse Fc gamma receptors, MAbs Jul. 9 (5) (2017), https://doi.org/10.1080/19420862.2017.1323159.

[7] G. Dekkers, L. Treffers, R. Plomp, A.E.H. Bentlage, M. de Boer, C.A.M. Koeleman, S. N. Lissenberg-Thunnissen, R. Visser, M. Brouwer, J.Y. Mok, et al., Decoding the Human Immunoglobulin G-Glycan Repertoire Reveals a Spectrum of Fc-Receptor- and Complement-Mediated-Effector Activities, Front Immunol. 8 (2017), https://doi.org/10.3389/fimmu.2017.00877.

[8] J. Dunbar, K. Krawczyk, J. Leem, C. Marks, J. Nowak, C. Regep, G. Georges, S. Kelm, B. Popovic, C.M. Deane, SAbPred: a structure-based antibody prediction server, Nucleic Acids Res 44 (2016) W474–W478, https://doi.org/10.1093/NAR/GKW361.

[9] EMA Guidance 3AB4a, Production and Quality Control of Monoclonal Antibodies" (Last Updated July 1995), European Medicines Agency (EMA), London, United Kingdom, 1995. ⟨https://www.ema.europa.eu/en/documents/scientific-guideline/production-quality-control-monoclonal-antibodies_en.pdf⟩. Retrieved 20/09/2022 from.

[10] T. Fiolet, Y. Kherabi, C.J. MacDonald, J. Ghosn, N. Peiffer-Smadja, Comparing COVID-19 vaccines for their characteristics, efficacy and effectiveness against SARS-CoV-2 and variants of concern: a narrative review, Clin. Microbiol. Infect. 28 (2022) 202–221, https://doi.org/10.1016/j.cmi.2021.10.005.

[11] J. Freeth, J. Soden, New Advances in Cell Microarray Technology to Expand Applications in Target Deconvolution and Off-Target Screening, SLAS Discov. 25 (2020) 223–230, https://doi.org/10.1177/2472555219897567.

[12] T. Hageman, H. Wei, P. Kuehne, J. Fu, R. Ludwig, L. Tao, A. Leone, M. Zocher, T. K. Das, Impact of Tryptophan Oxidation in Complementarity-Determining Regions of Two Monoclonal Antibodies on Structure-Function Characterized by Hydrogen-Deuterium Exchange Mass Spectrometry and Surface Plasmon Resonance, Pharm. Res 36 (2018), https://doi.org/10.1007/S11095-018-2545-8.

[13] W. Hübner, P. Chen, A.Del Portillo, Y. Liu, R.E. Gordon, B.K. Chen, Sequence of human immunodeficiency virus type 1 (HIV-1) Gag localization and oligomerization monitored with live confocal imaging of a replication-competent, fluorescently tagged HIV-1, J. Virol. 81 (2007) 12596–12607, https://doi.org/10.1128/JVI.01088-07.

[14] N. Izquierdo-Useros, J. Blanco, I. Erkizia, M.T. Fernández-Figueras, F.E. Borràs, M. Naranjo-Gómez, M. Bofill, L. Ruiz, B. Clotet, J. Martinez-Picado, et al., Maturation of Blood-Derived Dendritic Cells Enhances Human Immunodeficiency Virus Type 1 Capture and Transmission, J. Virol. 81 (2007) 7559–7570, https://doi.org/10.1128/JVI.02572-06.

[15] N. Izquierdo-Useros, M. Lorizate, F.-X.X. Contreras, M.T. Rodriguez-Plata, B. Glass, I. Erkizia, J.G. Prado, J. Casas, G. Fabriàs, H.-G.G. Kräusslich, et al., Sialyllactose in viral membrane gangliosides is a novel molecular recognition pattern for mature dendritic cell capture of HIV-1, PLoS Biol. 10 (2012) e1001315, https://doi.org/10.1371/journal.pbio.1001315.

[16] N. Izquierdo-Useros, M. Lorizate, M.C. Puertas, M.T. Rodriguez-Plata, N. Zangger, E. Erikson, M. Pino, I. Erkizia, B. Glass, B. Clotet, et al., Siglec-1 Is a Novel Dendritic Cell Receptor That Mediates HIV-1 Trans-Infection Through Recognition of Viral Membrane Gangliosides, PLoS Biol. 10 (2012) e1001448, https://doi.org/10.1371/journal.pbio.1001448.

[17] F.A. Lempp, L. Soriaga, M. Montiel-Ruiz, F. Benigni, J. Noack, Y.-J. Park, S. Bianchi, A.C. Walls, J.E. Bowen, J. Zhou, et al., Lectins enhance SARS-CoV-2 infection and influence neutralizing antibodies, Nature (2021), https://doi.org/10.1038/s41586-021-03925-1.

[18] X. Lu, R.P. Nobrega, H. Lynaugh, T. Jain, K. Barlow, T. Boland, A. Sivasubramanian, M. Vásquez, Y. Xu, Deamidation and isomerization liability analysis of 131 clinical-stage antibodies, MAbs 11 (2019) 45, https://doi.org/10.1080/19420862.2018.1548233.

[19] X. Lu, R.P. Nobrega, H. Lynaugh, T. Jain, K. Barlow, T. Boland, A. Sivasubramanian, M. Vásquez, Y. Xu, Development of therapeutic antibodies for the treatment of diseases, J. Biomed. Sci. 2020 27:1 27 (2020) 1–30, https://doi.org/10.1186/S12929-019-0592-Z.

[20] Q. Luo, M.K. Joubert, R. Stevenson, R.R. Ketchem, L.O. Narhi, J. Wypych, Chemical modifications in therapeutic protein aggregates generated under different stress conditions, J. Biol. Chem. 286 (2011) 25134–25144, https://doi.org/10.1074/JBC.M110.160440.

[21] J. Martinez-Picado, P.J. McLaren, I. Erkizia, M.P. Martin, S. Benet, M. Rotger, J. Dalmau, D. Ouchi, S.M. Wolinsky, S. Penugonda, et al., Identification of Siglec-1 null individuals infected with HIV-1, Nat. Commun. 7 (2016) 12412, https://doi.org/10.1038/ncomms12412.

[22] J.A. Pavon, L. Xiao, X. Li, J. Zhao, D. Aldredge, E. Dank, A. Fridman, Y.H. Liu, Selective Tryptophan Oxidation of Monoclonal Antibodies: Oxidative Stress and Modeling Prediction, Anal. Chem. 91 (2019) 2192–2200, https://doi.org/10.1021/ACS.ANALCHEM.8B04768.

[23] D. Perez-Zsolt, I. Erkizia, M. Pino, M. García-Gallo, M.T. Martin, S. Benet, J. Chojnacki, M.T. Fernández-Figueras, D. Guerrero, V. Urrea, et al., Anti-Siglec-1 antibodies block Ebola viral uptake and decrease cytoplasmic viral entry, Nat. Microbiol 4 (2019) 1558–1570, https://doi.org/10.1038/s41564-019-0453-2.

[24] D. Perez-Zsolt, J. Martinez-Picado, N. Izquierdo-Useros, When dendritic cells go viral: The role of Siglec-1 in host defense and dissemination of enveloped viruses, Viruses 12 (2019) 1–19, https://doi.org/10.3390/v12010007.

[25] D. Perez-Zsolt, J. Muñoz-Basagoiti, J. Rodon, M. Elosua-Bayes, D. Raïch-Regué, C. Risco, M. Sachse, M. Pino, S. Gumber, M. Paiardini, et al., SARS-CoV-2 interaction with Siglec-1 mediates trans-infection by dendritic cells, Cell Mol. Immunol. 18 (2021) 2676–2678, https://doi.org/10.1038/s41423-021-00794-6.

[26] S. Prenzler, S. Rudrawar, M. Waespy, S. Kelm, S. Anoopkumar-Dukie, T. Haselhorst, The role of sialic acid-binding immunoglobulin-like-lectin-1 (siglec-1) in immunology and infectious disease, Int Rev. Immunol. 42 (2) (2023), https://doi.org/10.1080/08830185.2021.1931171.

[27] W.B. Puryear, H. Akiyama, S.D. Geer, N.P. Ramirez, X. Yu, B.M. Reinhard, S. Gummuluru, Interferon-Inducible Mechanism of Dendritic Cell-Mediated HIV-1 Dissemination Is Dependent on Siglec-1/CD169, PLoS Pathog. 9 (2013), https://doi.org/10.1371/journal.ppat.1003291.

[28] H. Qiu, R. Wei, J. Jaworski, E. Boudanova, H. Hughes, S. VanPatten, A. Lund, J. Day, Y. Zhou, T. McSherry, et al., Engineering an anti-CD52 antibody for enhanced deamidation stability, MAbs 11 (2019) 1266–1275, https://doi.org/10.1080/19420862.2019.1631117.

[29] D. Raïch-Regué, P. Resa-Infante, M. Gallemí, F. Laguia, X. Muñiz-Trabudua, J. Muñoz-Basagoiti, D. Perez-Zsolt, J. Chojnacki, S. Benet, B. Clotet, et al., Role of Siglecs in viral infections: A double-edged sword interaction, Mol. Asp. Med (2022) 101113, https://doi.org/10.1016/j.mam.2022.101113.

[30] X. Sewald, M.S. Ladinsky, P.D. Uchil, J. Beloor, R. Pi, C. Herrmann, N. Motamedi, T.T. Murooka, M.A. Brehm, D.L. Greiner, et al., Retroviruses use CD169-mediated trans-infection of permissive lymphocytes to establish infection, Science 350 (1979) (2015) 563–567, https://doi.org/10.1126/science.aab2749.
[31] Taylor B.S., Tieu H.-V., Jones J. & Wilkin T.J. Clinical Trials and Investigational Antiretroviral Agents Possible Cure of HIV-1 Infection CROI 2019: Advances in Antiretroviral Therapy, n.d.
[32] T. Vink, M. Oudshoorn-Dickmann, M. Roza, J.J. Reitsma, R.N. de Jong, A simple, robust and highly efficient transient expression system for producing antibodies, Methods 65 (2014) 5–10, https://doi.org/10.1016/J.YMETH.2013.07.018.
[33] A.A. Wakankar, R.T. Borchardt, C. Eigenbrot, S. Shia, Y.J. Wang, S.J. Shire, J. L. Liu, Aspartate isomerization in the complementarity-determining regions of two closely related monoclonal antibodies, Biochemistry 46 (2007) 1534–1544, https://doi.org/10.1021/BI061500T.